

# PUBLISHED VERSION

Bo Xu, Cecilia Cheval, Anuphon Laohavisit, Bradleigh Hocking, David Chiasson, Tjelvar S. G. Olsson, Ken Shirasu, Christine Faulkner and Matthew Gilliam

**A calmodulin-like protein regulates plasmodesmal closure during bacterial immune responses**  
New Phytologist, 2017; 215(1):77-84

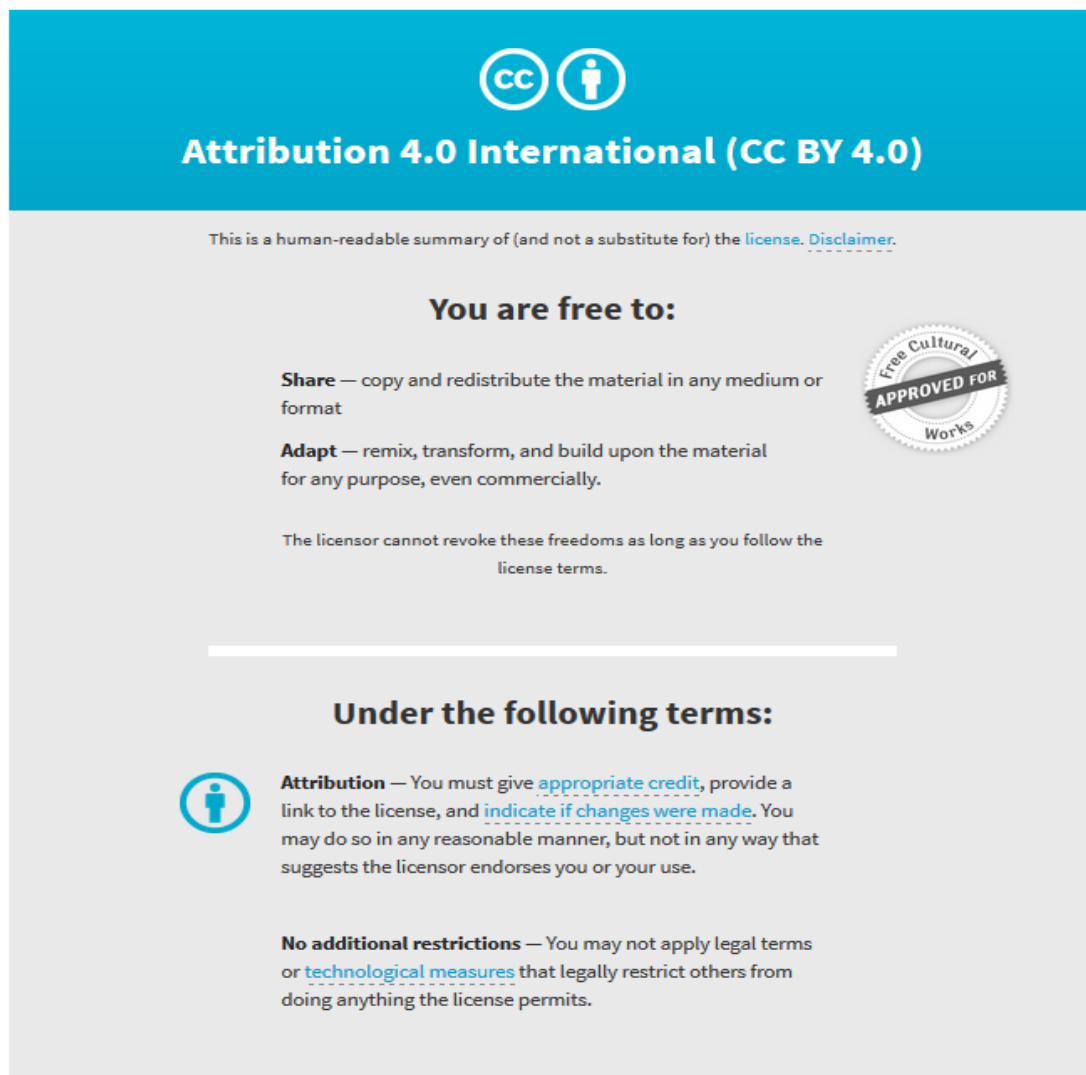
© 2017 The Authors. New Phytologist © 2017 New Phytologist Trust This is an open access article under the terms of the Creative Commons Attribution License, which permits use, distribution and reproduction in any medium, provided the original work is properly cited.

Originally published at:

<http://doi.org/10.1111/nph.14599>

## PERMISSIONS

<http://creativecommons.org/licenses/by/4.0/>



The image shows the Creative Commons Attribution 4.0 International (CC BY 4.0) license graphic. It features a blue header with the CC logo and the text "Attribution 4.0 International (CC BY 4.0)". Below the header, there is a disclaimer: "This is a human-readable summary of (and not a substitute for) the [license](#). [Disclaimer](#)." The main content is divided into two sections: "You are free to:" and "Under the following terms:". The "You are free to:" section lists "Share" (copy and redistribute) and "Adapt" (remix, transform, and build upon) with a "Free Cultural Works APPROVED FOR" seal. The "Under the following terms:" section lists "Attribution" (give credit, link to license, indicate changes) and "No additional restrictions" (no legal terms or technological measures).

**Attribution 4.0 International (CC BY 4.0)**

This is a human-readable summary of (and not a substitute for) the [license](#). [Disclaimer](#).

**You are free to:**

**Share** — copy and redistribute the material in any medium or format

**Adapt** — remix, transform, and build upon the material for any purpose, even commercially.

The licensor cannot revoke these freedoms as long as you follow the license terms.

**Under the following terms:**

**Attribution** — You must give [appropriate credit](#), provide a link to the license, and [indicate if changes were made](#). You may do so in any reasonable manner, but not in any way that suggests the licensor endorses you or your use.

**No additional restrictions** — You may not apply legal terms or [technological measures](#) that legally restrict others from doing anything the license permits.

1 August 2017

<http://hdl.handle.net/2440/106051>

## Rapid report

## A calmodulin-like protein regulates plasmodesmal closure during bacterial immune responses

Authors for correspondence:

Matthew Gilliham

Tel: +61 8 8313 8145

Email: matthew.gilliham@adelaide.edu.au

Christine Faulkner

Tel: +44 1603 450 000

Email: christine.faulkner@jic.ac.uk

Received: 8 December 2016

Accepted: 10 April 2017

Bo Xu<sup>1,2\*</sup>, Cécilia Cheval<sup>3\*</sup>, Anuphon Laohavisit<sup>4\*</sup>, Bradleigh Hocking<sup>1,2</sup>, David Chiasson<sup>2</sup>, Tjelvar S. G. Olsson<sup>3</sup>, Ken Shirasu<sup>4</sup>, Christine Faulkner<sup>3\*</sup> and Matthew Gilliham<sup>1,2\*</sup>

<sup>1</sup>Australian Research Council Centre of Excellence in Plant Energy Biology, Waite Research Institute, University of Adelaide, Glen Osmond, SA 5064, Australia; <sup>2</sup>School of Agriculture, Food and Wine, Waite Research Institute, University of Adelaide, Glen Osmond, SA 5064, Australia; <sup>3</sup>John Innes Centre, Norwich Research Park, Colney Lane, Norwich, NR4 7UH, UK; <sup>4</sup>RIKEN Centre for Sustainable Resource Science, Tsurumi-ku, Yokohama 230-0045, Japan

*New Phytologist* (2017) **215**: 77–84  
doi: 10.1111/nph.14599

**Key words:** At3g50770, biotic stress, cell-to-cell communication, electrophoresis mobility shift, maltose-binding protein, pathogen-associated molecular pattern (PAMP).

## Summary

- Plants sense microbial signatures via activation of pattern recognition receptors (PPRs), which trigger a range of cellular defences. One response is the closure of plasmodesmata, which reduces symplastic connectivity and the capacity for direct molecular exchange between host cells.
- Plasmodesmal flux is regulated by a variety of environmental cues but the downstream signalling pathways are poorly defined, especially the way in which calcium regulates plasmodesmal closure.
- Here, we identify that closure of plasmodesmata in response to bacterial flagellin, but not fungal chitin, is mediated by a plasmodesmal-localized Ca<sup>2+</sup>-binding protein Calmodulin-like 41 (CML41). *CML41* is transcriptionally upregulated by flg22 and facilitates rapid callose deposition at plasmodesmata following flg22 treatment. *CML41* acts independently of other defence responses triggered by flg22 perception and reduces bacterial infection.
- We propose that *CML41* enables Ca<sup>2+</sup>-signalling specificity during bacterial pathogen attack and is required for a complete defence response against *Pseudomonas syringae*.

## Introduction

Plasmodesmata are plasma membrane-lined pores that connect the cytoplasm of adjoining plant cells, allowing the passage of small molecules and ions through the plant symplast (Lucas & Lee, 2004). Our understanding of plasmodesmata has grown in the last decade (Lucas & Lee, 2004; Lee & Lu, 2011; Han & Kim, 2016; Tilsner *et al.*, 2016). For instance, it is now clear that plasmodesmata dynamically regulate cell-to-cell connectivity during developmental transitions and in response to environmental change, e.g. the down-regulation of plasmodesmal flux is an essential defence response following pathogen attack (Lee *et al.*, 2011; Faulkner *et al.*, 2013).

Bacterial flagellin triggers many defence responses via the perception of the immunogenic peptide of flagellin (flg22) by its cognate receptor FLS2 (Gómez-Gómez & Boller, 2000). In

*Arabidopsis* these responses include both the influx of Ca<sup>2+</sup> and plasmodesmal closure; Ca<sup>2+</sup> signalling is believed to be a critical component of a successful immune response (Lecourieux *et al.*, 2006; Seybold *et al.*, 2014). Previous studies have shown that changes in cytosolic Ca<sup>2+</sup> concentration close plasmodesmata (Tucker & Boss, 1996; Holdaway-Clarke *et al.*, 2000) – this has led to speculation that Ca<sup>2+</sup> signals regulate plasmodesmal flux following pathogen perception (e.g. Han & Kim, 2016; Tilsner *et al.*, 2016). While plasmodesmata-located calcium responsive proteins and putative calmodulin-binding sites have been identified (Baluška *et al.*, 1999; Chen *et al.*, 2005; Fernandez-Calvino *et al.*, 2011; Vaddepalli *et al.*, 2014) none have been characterized for their specific role in plasmodesmal function.

Here, we identify Calmodulin-like protein 41 (*CML41*) as a plasmodesmata-located, Ca<sup>2+</sup> responsive protein that mediates flg22-induced callose-dependent plasmodesmal closure. *CML41* expression is upregulated by flg22 and positively regulates defence

\*These authors contributed equally to this work.

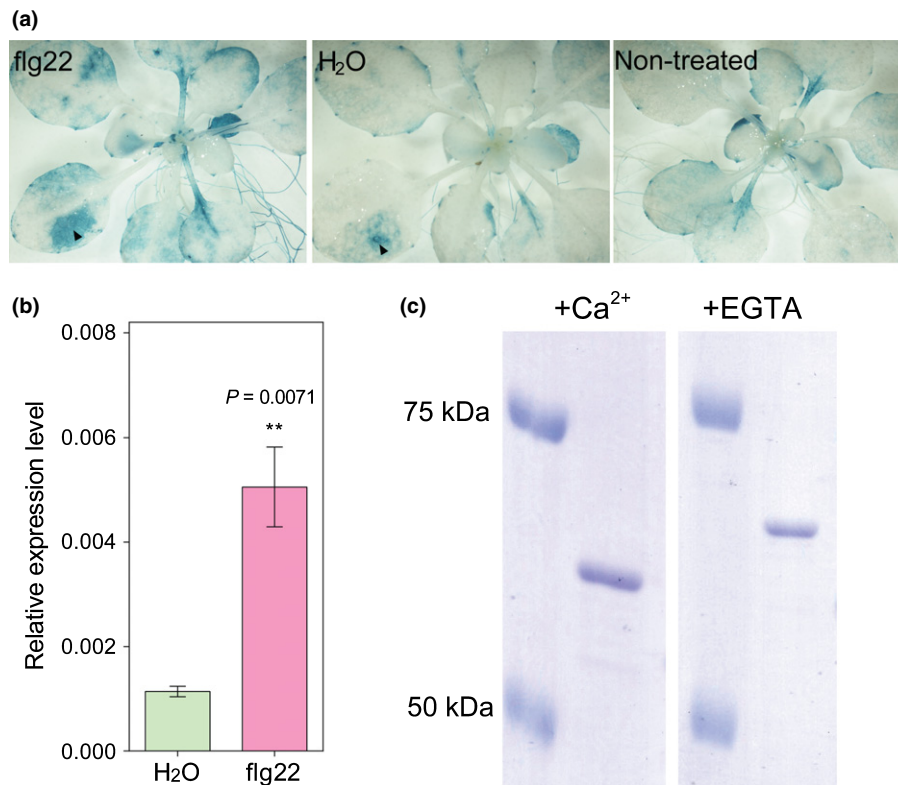


**Fig. 1** *CML41* is induced by flg22 in leaves and binds  $\text{Ca}^{2+}$ . (a) GUS histochemical staining of 24-d-old *proCML41::GUS* plants treated with either H<sub>2</sub>O or flg22 infiltration for 4 h, as well as nontreatment control as indicated. Both flg22 and H<sub>2</sub>O injection at the wound/infiltration site is indicated by arrowheads, there was a localized increase in GUS activity induced by both flg22 and H<sub>2</sub>O injection at the wound site. (b) Quantitative RT-PCR analysis of *CML41* in the leaves of 5–6-wk-old wildtype *Arabidopsis* Col-0 plants grown in short-day conditions (with 9 h : 15 h, light : dark) pre-infiltrated with either H<sub>2</sub>O (green) or 1  $\mu\text{M}$  flg22 (magenta) for 12 h. Gene transcript level was relative to *GAPDH-A* (At3g26650). Data represent the mean  $\pm$  standard error of the mean (SEM),  $n = 3$  biological replicates. Primer pairs used for (b) listed in Supporting Information Table S1. Statistical difference was determined by Student's *t*-test, asterisks indicate statistical significance, *P*-value as indicated. (c) Gel shift  $\text{Ca}^{2+}$  binding assay, purified recombinant MBP-*CML41* protein was separated on 8% SDS-PAGE gel in the presence of 1 mM  $\text{CaCl}_2$  or 10 mM EGTA, the mobility of proteins was determined by comparison with the Precision Plus Protein™ Standards as indicated.

against *Pseudomonas syringae*; therefore, we have identified a novel component of plant defence that links  $\text{Ca}^{2+}$  signals with callose deposition and plasmodesmata closure.

## Materials and Methods

### Plant material and growth conditions

*Arabidopsis thaliana* ecotype Col-0 and transgenic plants were grown in soil under short day conditions (9 h : 15 h, light : dark, 22°C) for 5–6 wk (Conn *et al.*, 2013), unless indicated otherwise.

### Gene cloning and plasmid construction

The coding sequence of *CML41* (At3g50770) with or without a stop codon was cloned via PCR (Phusion™ Hot Start High-Fidelity DNA polymerase; Finnzymes, Vantaa, Finland) with the primers listed in Supporting Information Table S1. To silence *CML41*, an artificial micro RNA (amiRNA, 5'-TAAACCGT CATCATTTGACCA-3') was designed against the *CML41* mRNA sequence using Web Micro RNA Designer (WMD3, <http://wmd3.weigelworld.org/cgi-bin/webapp.cgi>) (Schwab *et al.*,

2006). Whilst a 2-kb sequence upstream from the *CML41* ATG start codon was amplified by PCR to represent the *CML41* promoter (*proCML41*). All these PCR products were cloned via the Gateway® system (Invitrogen, Thermo Fisher Scientific, Waltham, MA, USA) following the manufacturers' instructions. The *CML41* gene with a stop codon was recombined into pDEST566 for protein expression in *Escherichia coli* and into the binary vector pMDC32 for plant overexpression. *CML41* without the stop codon was recombined into the binary vector pMDC83 containing a green fluorescent protein (GFP) tag on the C-terminus for protein localization and *CML41-amiRNA* was recombined into the binary vector pMDC32 for knockdown of *CML41* in the plant. The *proCML41* was recombined into the binary vector pMDC162 for a GUS histochemical assay (Curtis & Grossniklaus, 2003) and *35S:PDLPI-mCherry* was made by Golden Gate cloning. Stable transformation of *Arabidopsis* was performed by floral dip and T3 homozygote plants were used for all experiments.

### Subcellular localization

Ectopically expressed fluorescent proteins in transgenic *Arabidopsis* plants were imaged using a confocal laser scanning microscope

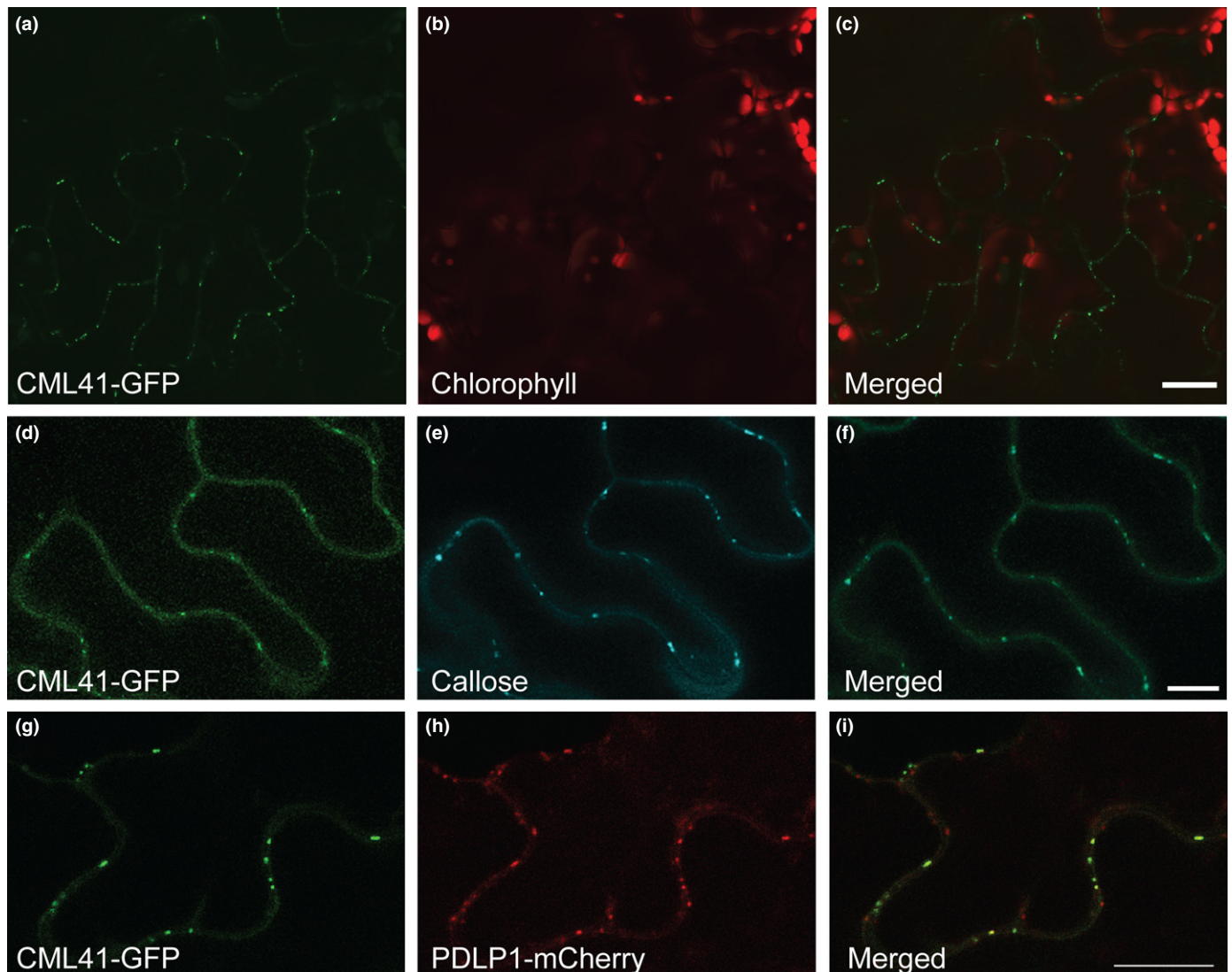


**Fig. 2** CML41 localizes to plasmodesmata. (a–c) Confocal image of CML41 tagged with GFP in the leaves of 5–6-wk-old *35S::CML41-GFP Arabidopsis* plant; bars, 20  $\mu\text{m}$ . (d–f) Co-localization of CML41-GFP (d) with callose stained by aniline blue (e) in the leaves of 5–6-wk-old *35S::CML41-GFP Arabidopsis* leaf; bars, 10  $\mu\text{m}$ . (g–i) Co-localization of CML41-GFP (g) with PDLP1-mCherry (h), transiently expressed in *Nicotiana benthamiana*; bars, 10  $\mu\text{m}$ .

equipped with a Zeiss Axioskop 2 mot plus LSM5 PASCAL and argon laser (Carl Zeiss, Oberkochen, Germany) or a Leica SP5 confocal microscope (Leica Microsystems, Wexlar, Germany). Sequential scanning and laser excitation was used to capture fluorescence from GFP (excitation = 488 nm, emission = 505–530 nm), aniline blue (excitation = 405 nm, emission = 440–490 nm) and mCherry (excitation = 561 nm, emission = 600–640 nm).

#### GUS histochemical analysis

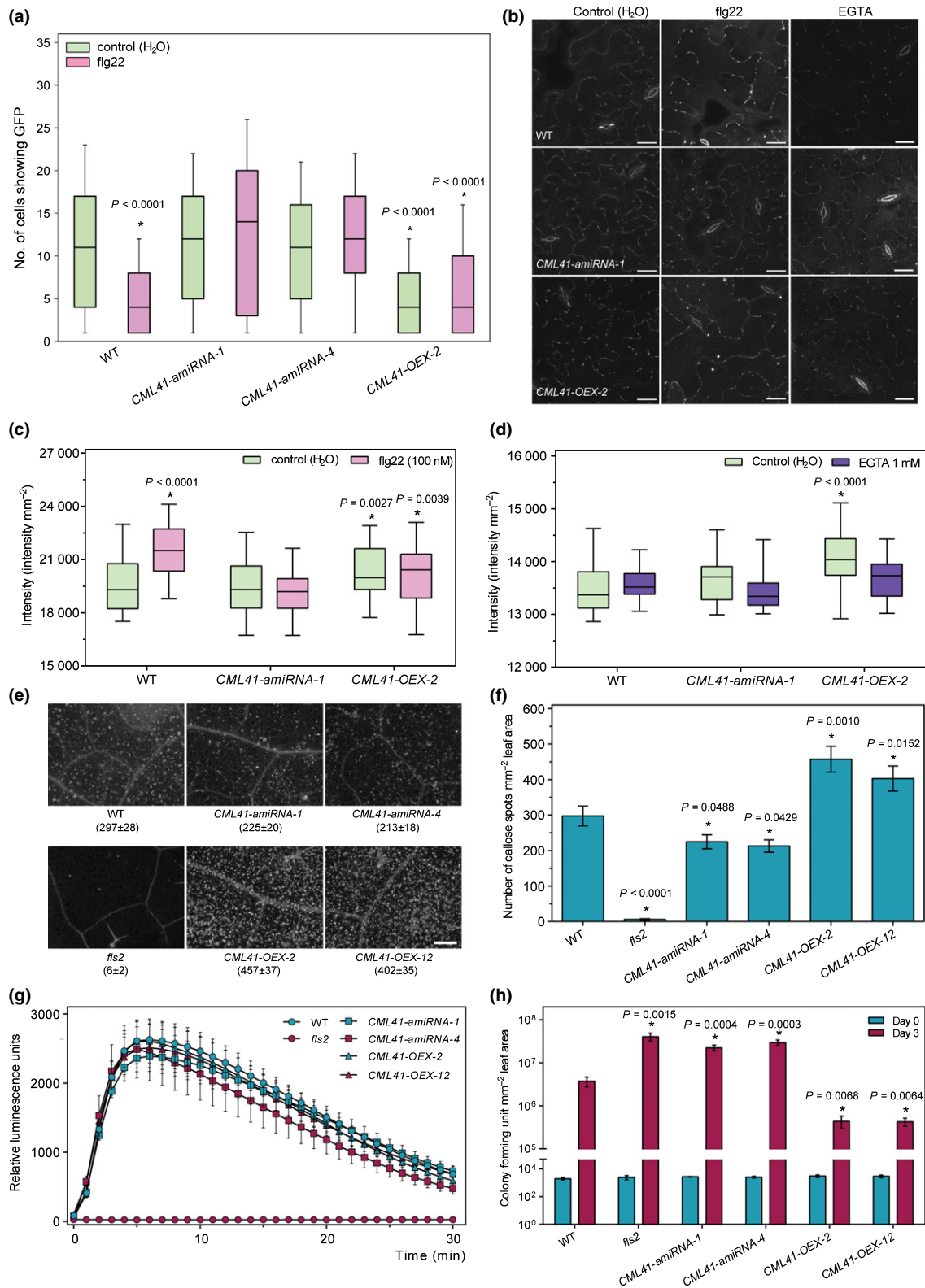
Transgenic *proCML41::GUS* plants were stained in the dark using a buffer containing 50 mM sodium phosphate pH = 7.0, 10 mM EDTA, 2 mM potassium ferrocyanide, 2 mM potassium ferricyanide, 0.1% (v/v) Triton X-100, 0.1% (w/v) X-Gluc (5-bromo-4-chloro-3-indolyl  $\beta$ -D-glucuronide) vacuum infiltrated for 15 min, followed by a 3 h incubation at 37°C. The plants were cleared of chlorophyll in 70% ethanol and imaged using a SMZ800 Stereo Fluorescence microscope (Nikon, Tokyo, Japan).

#### Quantitative RT-PCR analysis

RNA was extracted from leaves using TRIzol (Invitrogen) and treated with Turbo DNA-free kit (Ambion, Thermo Fisher Scientific) before cDNA synthesis using SuperScript<sup>®</sup> III Reverse Transcriptase (Invitrogen). Quantitative reverse transcription polymerase chain reaction (RT-PCR) was performed on the cDNA samples with primers listed in Table S1 using the fluorescence output from a QuantStudio<sup>™</sup> 12K Flex Real-Time PCR System. Quantitative RT-PCR analysis via the  $2^{-\Delta\text{Ct}}$  method to calculate the gene expression level relative to either *GAPDH-A* (At3g26650) or *UBI10* (At4g05320) as an internal control (Schmittgen & Livak, 2008).

#### Electrophoresis mobility shift assays

Recombinant *CML41* was expressed in T7 Expression *lysY11<sup>q</sup>* *E. coli* cells (New England Biolabs, Ipswich, MA, USA) using a



pDEST566 vector tagged with a 6×His maltose-binding protein (MBP) to enhance solubility of CML41 (Kapust & Waugh, 1999). The recombinant CML41 was purified using Poly-Prep<sup>®</sup> Chromatography Columns (Bio-Rad, Hercules, CA, USA) and Talon<sup>®</sup>

Metal Affinity Resin (Clontech, Mountain View, CA, USA) and desalted using Zeba<sup>™</sup> Spin Desalting Columns (Thermo Fisher Scientific) following the manufacturers' guide. The electrophoresis mobility shift assay was optimized from methods previously

**Fig. 3** CML41 negatively modulates plasmodesmatal permeability and positively regulates callose production and plant defence. (a) Plasmodesmata permeability of wildtype (WT) *Arabidopsis* and CML41 transgenic lines (CML41-amiRNA-1, -4 and CML41-OEX-2) in response to 100 nM flg22. Plants were bombarded with constructs capable of producing GFP. Diffusion of GFP to surrounding cells provided a measure of molecular flux through plasmodesmata. Plants were infiltrated with flg22 2 h after bombardment. In each box-plot, the white line indicates the median value, the shaded area represents the lower and upper quartiles, and the error bars indicate the minimum and maximum values,  $n = 187$  cells for WT (control), 137 for WT (flg22), 85 for CML41-amiRNA-1 (control), 103 for CML41-amiRNA-1 (flg22), 145 for CML41-amiRNA-4 (control), 163 for CML41-amiRNA-1 (flg22), 666 for CML41-OEX-2 (control) and 198 for CML41-OEX-2 (flg22). Statistical difference from the WT control was determined by Student's *t*-test, asterisks indicate statistical significance, *P*-values as indicated. (b) Confocal images of aniline blue stained plasmodesmal callose in the leaves of 5–6-wk-old *Arabidopsis* WT, CML41-OEX-2 and CML41-amiRNA-1 lines upon H<sub>2</sub>O, flg22 and EGTA treatment for 30 min; bars, 20  $\mu$ m. (c, d) Quantification of PD callose fluorescence intensity in the leaves of 5–6-wk-old *Arabidopsis* WT, CML41-OEX-2 and CML41-amiRNA-1 lines following flg22 (c) and EGTA treatment (d). Box plots in (c) and (d) are as mentioned earlier,  $n = 24$  (c) and 27 (d). Statistical difference from the WT control was determined by Student's *t*-test, asterisks indicate statistical significance, *P*-values as indicated. (e) Macroscopy images and (f) quantification of callose deposition upon flg22 or H<sub>2</sub>O treatments in WT Col-0, *fls2*, CML41-amiRNA-1, -4 and CML41-OEX-2, -12 lines upon 1  $\mu$ M flg22 for 24 h, as indicated; bars, 200  $\mu$ m in (e). Data represent the mean  $\pm$  SEM,  $n = 18$  leaves. Statistical difference as determined by one-way analysis of variance (ANOVA), asterisks indicate statistical significance, *P*-values as indicated. (g) Reactive oxygen species (ROS) production stimulated by 1  $\mu$ M flg22 was monitored in *Arabidopsis* WT, *fls2*, CML41-amiRNA-1, -4 and CML41-OEX-2, -12 leaf discs recorded at every minute using a luminol assay in a microplate reader, *fls2* was used as a control. Data are given as relative luminescence units and represent in mean  $\pm$  SEM, from three independent trials with six technical replicates per biological replicate,  $n = 6$ . (h) Evaluation of CML41 transgenic plant susceptibility to *Pst* DC3000 *cor*<sup>-</sup>; quantification of bacterial growth in *fls2*, CML41-amiRNA-1, -4, CML41-OEX-2, -12 lines and *Arabidopsis* WT plants upon 0 and 3 d post-inoculation of *Pst* DC3000 *cor*<sup>-</sup> suspension. The bacterial colony number was counted in colony-forming unit (CFU) per cm<sup>2</sup>. Data represent mean  $\pm$  SEM,  $n = 6$ . Statistical difference as determined by multiple Student's *t*-test, asterisks indicate statistical significance from WT control or flg22 treated, *P*-values as indicated. The experiments were repeated three times with similar results. See Supporting Information Fig. S7 for the equivalent assays using *Pst* DC3000.

described (Garrigos *et al.*, 1991). Either 1 mM CaCl<sub>2</sub> or 10 mM EGTA (ethylene glycol-bis( $\beta$ -aminoethyl ether)-*N,N,N',N'*-tetraacetic acid) was added to the purified desalted recombinant protein samples. These samples were heated at 95°C for 2 min before electrophoresis separation on an 8% SDS-PAGE gel containing either 1 mM CaCl<sub>2</sub> or 10 mM EGTA. The mobility of proteins was determined by comparison with the Precision Plus Protein™ Standards (Bio Rad).

#### Plasmodesmal callose staining assay

The eighth rosette leaf was infiltrated with ultrapure water, or ultrapure water containing 100 nM flg22 or 1 mM EGTA for 30 min, followed by an infiltration of aniline blue (0.01% (w/v) in PBS buffer, pH 7.4). Callose deposits were imaged from the abaxial side of the leaf using a SP5 confocal microscope (Leica) or a Nikon A1R laser scanning confocal with excitation = 405 nm and emission = 500–550 nm. Z-stack images were collected from 24 to 27 technical replicates from two independent biological replicates. Data from different microscopes was not pooled. Callose was quantified using automated image analysis. All annotated images were inspected before inclusion of any data in the statistical analysis. The image analysis pipeline was written in Python; image analysis scripts and further information are available under the open source MIT licence on GitHub (<https://github.com/JIC-CSB/find-plasmodesmata>).

#### Macroscopic callose deposition assay

Either ultrapure H<sub>2</sub>O or ultrapure H<sub>2</sub>O containing 1  $\mu$ M flg22 was infiltrated into rosette leaves. After 24 h, the infiltrated leaves were incubated in staining solution (150 mM sodium phosphate, 0.05% (w/v) aniline blue, pH = 8) for an additional 1 h in the dark. The stained leaves were mounted in 50% (v/v) glycerol and imaged with an Axiophot Photomicroscope excitation from a mercury light source and captured with a UV filter (LP = 470 nm) (Carl Zeiss).

Callose deposited in leaves was measured by IMAGEJ, using particle analysis (<http://rsbweb.nih.gov/ij/>).

#### Reactive oxygen species (ROS) burst assay

Leaf discs were obtained by using a 4 mm disposable biopsy punch (Kei Medical, Tokyo, Japan) and incubated overnight with 100  $\mu$ M L-012 (Wako Chemical, Osaka, Japan) in a Greiner 96 well white plate. Leaf discs were washed once with sterile deionized (DI) water and then triggered with 1  $\mu$ M flg22 and luminescence was measured for 30 min (Tristar<sup>2</sup> LB 942; Berthold Technologies, Bad Wilbad, Germany). The data was replicated three times in independent trials.

#### Bacterial growth assay

Bacterial growth assays were performed as described previously (Kadota *et al.*, 2014), with slight modification. We assessed the significance of CML41 activity in overall plant resistance by first infiltrating leaves of different *Arabidopsis* lines with the virulent bacterial pathogen *P. syringae* pv. *tomato* (*Pst*) DC3000 (OD = 0.0002). We next performed infections by surface inoculation with the less virulent, coronatine deficient strain DC3000 (*cor*<sup>-</sup>). Briefly, *Pst* bacterial suspension with OD<sub>600 nm</sub> = 0.2 in 0.02% Silwet L-77 were generously sprayed onto leaf abaxial and adaxial surfaces of 5–6-wk-old plants. Plants were covered during the course of infection and leaf discs were taken 3 h post-inoculation (day 0) or 3 d post-inoculation (day 3) from three leaves per plant, with six plants per genotype per independent trial. Bacterial growth was assessed by colony counting.

#### GFP bombardment assay

Microprojectile bombardment assays were performed as previously described (Faulkner *et al.*, 2013). Bombardment sites were assessed by epifluorescence microscopy (Leica DM6000).

## Results and Discussion

The 50 members of the *CML* gene family of *A. thaliana* have been proposed to encode proteins that facilitate specificity during  $\text{Ca}^{2+}$  signalling (McCormack *et al.*, 2005; Bender & Snedden, 2013). *CML41* expression was previously shown to be upregulated by *flg22* (Denoux *et al.*, 2008), so we investigated whether it had a role in pathogen responses. First, we confirmed that *CML41* transcription was induced *flg22* using quantitative RT-PCR and expression analysis of the *CML41* promoter (Fig. 1a,b). We next investigated whether *CML41* could bind  $\text{Ca}^{2+}$  and, therefore, has the potential to decode *flg22*-induced  $\text{Ca}^{2+}$ -signals. CMLs can change conformation upon  $\text{Ca}^{2+}$  binding (Bender & Snedden, 2013), to test whether this is the case for *CML41* we performed an electrophoresis mobility shift assay (Garrigos *et al.*, 1991). Initial attempts to express and purify *CML41* in *E. coli* were unsuccessful as the purified *CML41* was insoluble. Therefore, *CML41* was tagged with MBP to enhance its solubility and probed by western blot (Kapust & Waugh, 1999) (Fig. S1). The purified and soluble MBP-*CML41* fraction migrated faster in the presence of  $\text{Ca}^{2+}$  relative to EGTA (Fig. 1c), indicating its ability to bind  $\text{Ca}^{2+}$ . This result is consistent with the recent report that *CML41* binds to phenyl sepharose in a  $\text{Ca}^{2+}$ -dependent manner (Dell'Aglio *et al.*, 2016). Attempts to obtain the  $\text{Ca}^{2+}$ -binding affinity for *CML41* using microscale thermophoresis in a range of buffers were unsuccessful due to protein aggregation, even when tagged with MBP. However, the presence in *CML41* of EF-hands, which are conserved in other CML and have already been shown to bind  $\text{Ca}^{2+}$  in the nanomolar range, suggests that the  $\text{Ca}^{2+}$  responsiveness of *CML41* could have a physiological role (Fig. S2).

To investigate the subcellular localization of *CML41* we overexpressed *CML41* fused with *GFP* (*CML41-GFP*). In leaves, *CML41-GFP* localizes to punctate spots at the cell periphery (Fig. 2a–c), patterning that is reminiscent of plasmodesmata (Thomas *et al.*, 2008; Simpson *et al.*, 2009). We confirmed *CML41-GFP* was localized to plasmodesmata by co-staining plasmodesmal callose in Arabidopsis with aniline blue (Fig. 2d–f) or with Plasmodesmata-located Protein 1 (PDLP1) in *Nicotiana benthamiana* (Fig. 2g–i) (Thomas *et al.*, 2008). Plasmodesmal-association has not yet been observed for any other CMLs, suggesting a novel role for *CML41* of decoding *flg22*-induced  $\text{Ca}^{2+}$  signals at plasmodesmata (Bender & Snedden, 2013).

To further investigate the role of *CML41* at plasmodesmata, we generated *CML41* gain- and loss-of-function transgenic lines using either gene overexpression (OEX) or artificial micro RNA (amiRNA) as no T-DNA lines were available (Fig. S3). To determine whether *CML41* has a role in *flg22*-induced plasmodesmal closure we performed intercellular flux assays by measuring GFP diffusion from single cell transformation sites (Faulkner *et al.*, 2013). Whilst *flg22* treatment reduced spread of GFP in wildtype plants, indicating plasmodesmal closure, *CML41-amiRNA* lines did not close their plasmodesmata in response to *flg22* (Fig. 3a). *CML41-OEX* plants showed increased basal levels of plasmodesmal closure (reduced spread of GFP), which was unaffected by *flg22*-treatment (Fig. 3a).

To test whether *CML41*-mediated, *flg22*-induced plasmodesmal closure is executed by apoplastic callose deposition adjacent to plasmodesmata (Maule *et al.*, 2012), we used automated image analysis to quantify plasmodesmata-located aniline blue fluorescence. At 30 min post-treatment, plasmodesmal callose was significantly increased in wildtype plants (Fig. 3b,c), supporting a model where *flg22* induces plasmodesmal closure via rapid callose deposition. *CML41-amiRNA* lines showed no difference in callose deposition between  $\text{H}_2\text{O}$  and *flg22* treated tissue (Fig. 3b,c), which coincided with the loss of the plasmodesmal closure response in these plants (Fig. 3a). *CML41-OEX* plants had an increased presence of plasmodesmal callose in the basal state, which was reduced by the  $\text{Ca}^{2+}$ -chelator EGTA (Fig. 3b,d). These data indicate that  $\text{Ca}^{2+}$ -responsiveness of *CML41* is likely to play a critical and physiologically relevant role in *flg22*-induced plasmodesmal closure. Furthermore, this result implies that infiltration *per se* without EGTA (as performed in control experiments in Fig. 3a–f) may be sufficient to raise cytosolic  $\text{Ca}^{2+}$  concentration, as could be expected following a manipulation of the leaf apoplastic environment and water relations.

To examine whether *CML41* is involved more broadly in pathogen-associated molecular pattern (PAMP) responses we examined GFP movement in response to chitin, a fungal PAMP that reduces flux via plasmodesmata (Faulkner *et al.*, 2013). *CML41-amiRNA* plants showed the wildtype response to chitin (Fig. S4a); furthermore, chitin did not induce *CML41* transcription (Fig. S4b). This confirms that plants regulate plasmodesmal closure through different mechanisms following bacterial or fungal infection.

To assess *CML41* specificity to plasmodesmal function we examined other *flg22*-induced responses. Macroscopic callose deposition in the apoplast in response to *flg22* was detectable 24 h post-treatment (Gómez-Gómez *et al.*, 1999). In wildtype plants we observed widespread and greater callose deposition following *flg22* infiltration compared to water treatment (Figs 3e,f, S5) and the *fls2* control (Gómez-Gómez *et al.*, 1999). The *CML41-amiRNA* lines accumulated fewer callose deposits than wildtype plants after *flg22* treatment (Fig. 3e,f). *CML41-OEX* lines produced more callose deposits in response to *flg22* (Fig. 3e,f).

Reactive oxygen species (ROS) accumulate rapidly upon *flg22* treatment (Gómez-Gómez *et al.*, 1999; Boudsocq *et al.*, 2010). While *flg22*-induced ROS production is abolished in *fls2* (Gómez-Gómez *et al.*, 1999; Boudsocq *et al.*, 2010), it was observed at similar levels to wildtype in *CML41-amiRNA* and *CML41-OEX* plants (Fig. 3g) indicating that *CML41* does not play a role in *flg22*-induced ROS production. The *flg22* induces the expression of defence genes such as *flg22-induced Receptor Kinase 1* (*FRK1*), *cytochrome P450 monooxygenase* (*CYP81F2*) and *NDR1/HIN1-like 10* (*NHL10*) (Boudsocq *et al.*, 2010). All these genes were significantly up-regulated across all *flg22*-infiltrated plants (Fig. S6). Transcript abundance of the salicylic acid (SA) inducible gene, *PATHOGENESIS-RELATED 1* (*PRI*) (Wildermuth *et al.*, 2001; Zipfel *et al.*, 2004) is also enhanced by *flg22* and showed no obvious difference between *CML41* transgenic lines and wildtype plants within the same treatments (Fig. S6). This contrasts the action of *CML9* in the nucleus, which appears to negatively

regulate *PR1* expression and the deposition of callose during flg22 responses (Leba *et al.*, 2012). As the same transcriptional responses of these known early innate immunity induced genes are activated in wildtype, *CML41* overexpression and knockdown plants, this is strong evidence that CML41 does not work upstream of any of the corresponding response pathways.

In combination, this data establishes that CML41 functions in a specialized signalling pathway, downstream of FLS2 recognition of flg22. The localization of CML41 at plasmodesmata suggests that this signalling pathway directly regulates plasmodesmal function, closing the plasmodesmata within 30 min of pathogen perception (Fig. 3a). CML41 also functions in the production of large deposits of callose over a longer response timescale (Fig. 3e). It is not clear yet whether CML41 directly stimulates deposition via regulation of a callose synthase or inhibits a constitutive process of removal by interfering with  $\beta$ -1,3-glucanase activity (Luna *et al.*, 2011), this may become clearer when interacting partners are identified for CML41. It should be noted that we detected *CML41* expression in the roots following flg22 treatment (Fig. 1a); therefore, it is likely that CML41 plays a similar role in PD flux regulation when challenged with soil bacterial pathogens. An investigation is also warranted into: the role of CML41 in the other tissues in which it is expressed such as senescent leaves and flowers (McCormack *et al.*, 2005); and, the significance of its transcriptional regulation by RNA-dependent methylation (Baev *et al.*, 2010).

In this study we focused on assessing the significance of CML41 activity in overall plant resistance by surface inoculation of different *Arabidopsis* lines with *P. syringae* (Figs 3h, S6). Three days post-infection (3 dpi), *CML41-amiRNA* lines showed more bacterial growth than wildtype, similar to *fls2*, indicating they were more susceptible; while the *CML41-OEX* lines showed less bacterial growth than wildtype (Fig. 3h). This suggests that flg22-induced  $Ca^{2+}$  signalling via CML41 is a critical component of callose deposition. A parallel role for  $Ca^{2+}$  in a callose-independent plasmodesmal closure pathway has also been proposed (Sager & Lee, 2014); however, this does not appear to play a major role in the conditions assayed here.

We have identified CML41 as a  $Ca^{2+}$  responsive component of defensive plasmodesmal closure. Chitin-induced plasmodesmal closure has previously been shown to be critical to defence and overall resistance against a fungal pathogen and the data presented here identifies that flg22-induced plasmodesmal closure is similarly critical to defence against bacterial pathogens. Beyond establishing new understanding of the mechanisms of plasmodesmal function via  $Ca^{2+}$ , this highlights a role for symplastic connectivity in the full and complete execution of defence responses.

## Acknowledgements

The authors thank Dr Yasuhiro Kadota for critical review of the research, Dr Matthew Hartley for assistance with plasmodesmal image analysis, Roger Leigh, Steve Tyerman, Brent Kaiser, Matt Tucker and Rachel Burton for discussions. Epifluorescence and confocal microscopy were facilitated by access to the JIC Bioimaging and Computational Biology Platforms, respectively,

and Adelaide Microscopy. Funding: B.X. was supported by an University of Adelaide Graduate Research Scholarship; research was supported by the Australian Research Council through Centre of Excellence (CE140100008) and Future Fellowship (FT130100709) funding to M.G.; by the Biotechnology and Biological Sciences Research Council (BB/L000466/1) to C.F.; and by KAKENHI (24228008 and 15H05959) to K.S.

## Author contributions

M.G., C.F. and K.S. supervised the research. B.X. performed the majority of experiments except the following. B.H. cloned the amiRNA. B.X. and D.C. purified the protein and performed  $Ca^{2+}$  shift experiments. A.L. performed callose deposition, ROS burst and bacterial growth assays. C.C. performed bombardment assays and plasmodesmal callose quantification. T.S.G.O. wrote the image analysis script. C.C. and C.F. performed co-localization experiments. B.X., C.C., A.L., K.S., M.G. and C.F. drafted the manuscript. All authors commented on the manuscript.

## References

- Baev V, Naydenov M, Apostolova E, Ivanova D, Doncheva S, Minkov I, Yahubyan G. 2010. Identification of RNA-dependent DNA-methylation regulated promoters in *Arabidopsis*. *Plant Physiology and Biochemistry* 48: 393–400.
- Baluška F, Šamaj J, Napier R, Volkmann D. 1999. Maize calreticulin localizes preferentially to plasmodesmata in root apex. *Plant Journal* 19: 481–488.
- Bender KW, Snedden WA. 2013. Calmodulin-related proteins step out from the shadow of their namesake. *Plant Physiology* 163: 486–495.
- Boudsocq M, Willmann MR, McCormack M, Lee H, Shan L, He P, Bush J, Cheng S-H, Sheen J. 2010. Differential innate immune signalling via  $Ca^{2+}$  sensor protein kinases. *Nature* 464: 418–422.
- Chen M-H, Tian G-W, Gafni Y, Citovsky V. 2005. Effects of calreticulin on viral cell-to-cell movement. *Plant Physiology* 138: 1866–1876.
- Conn SJ, Hocking B, Dayod M, Xu B, Athman A, Henderson S, Aukett L, Conn V, Shearer MK, Fuentes S, Tyerman SD, Gilliam M. 2013. Protocol: optimising hydroponic growth systems for nutritional and physiological analysis of *Arabidopsis thaliana* and other plants. *Plant Methods* 9: 1.
- Curtis MD, Grossniklaus U. 2003. A gateway cloning vector set for high-throughput functional analysis of genes in *planta*. *Plant Physiology* 133: 462–469.
- Dell'Aglio E, Salvi D, Kraut A, Baudet M, Macherel D, Neveu M, Ferro M, Curien G, Rolland N. 2016. No plastidial calmodulin-like proteins detected by two targeted mass-spectrometry approaches and GFP fusion proteins. *New Negatives in Plant Science* 3: 19–26.
- Denoux C, Galletti R, Mammarella N, Gopalan S, Werck D, De Lorenzo G, Ferrari S, Ausubel FM, Dewdney J. 2008. Activation of defense response pathways by OGs and Flg22 elicitors in *Arabidopsis* seedlings. *Molecular Plant* 1: 423–445.
- Faulkner C, Petutschnig E, Benitez-Alfonso Y, Beck M, Robatzek S, Lipka V, Maule AJ. 2013. LYM2-dependent chitin perception limits molecular flux via plasmodesmata. *Proceedings of the National Academy of Sciences, USA* 110: 9166–9170.
- Fernandez-Calvino L, Faulkner C, Walshaw J, Saalbach G, Bayer E, Benitez-Alfonso Y, Maule A. 2011. *Arabidopsis* plasmodesmal proteome. *PLoS ONE* 6: e18880.
- Garrigos M, Deschamps S, Viel A, Lund S, Champeil P, Møller JV, le Maire M. 1991. Detection of  $Ca^{2+}$ -binding proteins by electrophoretic migration in the presence of  $Ca^{2+}$  combined with  $^{45}Ca^{2+}$  overlay of protein blots. *Analytical Biochemistry* 194: 82–88.
- Gómez-Gómez L, Boller T. 2000. FLS2: an LRR receptor-like kinase involved in the perception of the bacterial elicitor flagellin in *Arabidopsis*. *Molecular Cell* 5: 1003–1011.
- Gómez-Gómez L, Felix G, Boller T. 1999. A single locus determines sensitivity to bacterial flagellin in *Arabidopsis thaliana*. *Plant Journal* 18: 277–284.



- Han X, Kim J-Y. 2016. Integrating hormone- and micromolecule-mediated signaling with plasmodesmal communication. *Molecular Plant* 9: 46–56.
- Holdaway-Clarke TL, Walker NA, Hepler PK, Overall RL. 2000. Physiological elevations in cytoplasmic free calcium by cold or ion injection result in transient closure of higher plant plasmodesmata. *Planta* 210: 329–335.
- Kadota Y, Sklenar J, Derbyshire P, Stransfeld L, Asai S, Ntoukakis V, Jones JD, Shirasu K, Menke F, Jones A. 2014. Direct regulation of the NADPH oxidase RBOHD by the PRR-associated kinase BIK1 during plant immunity. *Molecular Cell* 54: 43–55.
- Kapust RB, Waugh DS. 1999. *Escherichia coli* maltose-binding protein is uncommonly effective at promoting the solubility of polypeptides to which it is fused. *Protein Science* 8: 1668–1674.
- Leba L-J, Perochon A, Cheval C, Ranty B, Galaud J-P, Aldon D. 2012. CML9, a multifunctional *Arabidopsis thaliana* calmodulin-like protein involved in stress responses and plant growth? *Plant Signaling & Behavior* 7: 1121–1124.
- Lecourieux D, Ranjeva R, Pugin A. 2006. Calcium in plant defence-signalling pathways. *New Phytologist* 171: 249–269.
- Lee J-Y, Lu H. 2011. Plasmodesmata: the battleground against intruders. *Trends in Plant Science* 16: 201–210.
- Lee J-Y, Wang X, Cui W, Sager R, Modla S, Czymbek K, Zybaliow B, van Wijk K, Zhang C, Lu H. 2011. A plasmodesmata-localized protein mediates crosstalk between cell-to-cell communication and innate immunity in *Arabidopsis*. *Plant Cell* 23: 3353–3373.
- Lucas WJ, Lee J-Y. 2004. Plasmodesmata as a supracellular control network in plants. *Nature Reviews Molecular Cell Biology* 5: 712–726.
- Luna E, Pastor V, Robert J, Flors V, Mauch-Mani B, Ton J. 2011. Callose deposition: a multifaceted plant defense response. *Molecular Plant-Microbe Interactions* 24: 183–193.
- Maule A, Faulkner C, Benitez-Alfonso Y. 2012. Plasmodesmata “in comunicado”. *Frontiers in Plant Science* 3: 30.
- McCormack E, Tsai Y-C, Braam J. 2005. Handling calcium signaling: arabidopsis CaMs and CMLs. *Trends in Plant Science* 10: 383–389.
- Sager R, Lee J-Y. 2014. Plasmodesmata in integrated cell signalling: insights from development and environmental signals and stresses. *Journal of Experimental Botany* 65: 6337–6358.
- Schmittgen TD, Livak KJ. 2008. Analyzing real-time PCR data by the comparative CT method. *Nature Protocols* 3: 1101–1108.
- Schwab R, Ossowski S, Riester M, Warthmann N, Weigel D. 2006. Highly specific gene silencing by artificial microRNAs in *Arabidopsis*. *Plant Cell* 18: 1121–1133.
- Seybold H, Trempel F, Ranf S, Scheel D, Romeis T, Lee J. 2014. Ca<sup>2+</sup> signalling in plant immune response: from pattern recognition receptors to Ca<sup>2+</sup> decoding mechanisms. *New Phytologist* 204: 782–790.
- Simpson C, Thomas C, Findlay K, Bayer E, Maule AJ. 2009. An *Arabidopsis* GPI-anchor plasmodesmal neck protein with callose binding activity and potential to regulate cell-to-cell trafficking. *Plant Cell* 21: 581–594.
- Thomas CL, Bayer EM, Ritzenthaler C, Fernandez-Calvino L, Maule AJ. 2008. Specific targeting of a plasmodesmal protein affecting cell-to-cell communication. *PLoS Biology* 6: e7.
- Tilsner J, Nicolas W, Rosado A, Bayer EM. 2016. Staying tight: plasmodesmal membrane contact sites and the control of cell-to-cell connectivity in plants. *Annual Review of Plant Biology* 67: 337–364.
- Tucker EB, Boss WF. 1996. Mastoparan-induced intracellular Ca<sup>2+</sup> fluxes may regulate cell-to-cell communication in plants. *Plant Physiology* 111: 459–467.
- Vaddepalli P, Herrmann A, Fulton L, Oelschner M, Hillmer S, Stratil TF, Fastner A, Hammes UZ, Ott T, Robinson DG. 2014. The C2-domain protein QUIRKY and the receptor-like kinase STRUBBELIG localize to plasmodesmata and mediate tissue morphogenesis in *Arabidopsis thaliana*. *Development* 141: 4139–4148.
- Wildermuth MC, Dewdney J, Wu G, Ausubel FM. 2001. Isochorismate synthase is required to synthesize salicylic acid for plant defence. *Nature* 414: 562–565.
- Zipfel C, Robatzek S, Navarro L, Oakeley EJ, Jones JD, Felix G, Boller T. 2004. Bacterial disease resistance in *Arabidopsis* through flagellin perception. *Nature* 428: 764–767.

## Supporting Information

Additional Supporting Information may be found online in the Supporting Information tab for this article:

**Fig. S1** CML41 was produced through heterologous expression in *Escherichia coli*.

**Fig. S2** *In silico* analysis of CML41 protein sequence and EF domains.

**Fig. S3** CML41 transcript abundance was modified in transgenic CML41 misexpression lines.

**Fig. S4** CML41 does not have a role in chitin response of plasmodesmata.

**Fig. S5** Callose production is not induced by water infiltration in CML41 overexpression or knockdown lines.

**Fig. S6** Early immune response gene transcription is not affected by CML41 overexpression or knockdown.

**Fig. S7** CML41 overexpression increases bacterial resistance.

**Table S1** Primers used for quantitative RT-PCR analysis and molecular cloning

Please note: Wiley Blackwell are not responsible for the content or functionality of any Supporting Information supplied by the authors. Any queries (other than missing material) should be directed to the *New Phytologist* Central Office.